Nanoscale Cellular Structures at Phase Boundaries of Ni-Cr-Al-Ti and Ni-Cr-Mo-Al-Ti Superalloys

CONG WANG and DAVID C. DUNAND

The microstructural evolution of Ni-20 pct Cr wires was studied during pack cementation where Al and Ti, with and without prior cementation with Mo, are deposited to the surface of the Ni-Cr wires and subsequently homogenized in their volumes. Mo deposition promotes the formation of Kirkendall pores and subsequent co-deposition of Al and Ti creates a triple-layered diffusional coating on the wire surface. Subsequent homogenization drives the alloying element to distribute evenly in the wires which upon further heat treatment exhibit the $\gamma + \gamma'$ superalloy structure. Unexpectedly, formation of cellular structures is observed at some of the boundaries between primary γ' grains and γ matrix grains. Based on additional features (*i.e.*, ordered but not perfectly periodic structure, confinement at $\gamma + \gamma'$ phase boundaries as a cellular film with ~100 nm width, as well as lack of topologically close-packed phases), and considering that similar, but much larger, microstructures were reported in commercial superalloys, it is concluded that the present cellular structure solidified as a thin film, composed of eutectic $\gamma + \gamma'$ and from which the γ' phase was subsequently etched, which was created by incipient melting of a region near the phase boundary with high solute segregation.

DOI: 10.1007/s11661-015-2831-6

I. INTRODUCTION

FOR many decades, the pack cementation technique has been actively employed and versatilely adapted in the superalloy industry for creating wear- and corrosion-resistant coatings geared toward high-demanding service environments. In general, pack cementation process involves four components, *i.e.*, substrate (Fe-, Co-, and Ni-base alloys), target alloying elements (Al, Cr, Si, *etc.*), activator (chloride and fluoride), and thermal ballast (inert Al_2O_3, ZrO_2, MgO, *etc.*). Upon heating in a flowing or static inert atmosphere to the desired temperature, alloying elements and halide powders react to form volatile metallic halides, which subsequently deposit onto the substrate surface and diffuse into the substrate, leading to the formation of phases and microstructures that protect the substrate.[1–3]

Previous studies have demonstrated the feasibility of alloying additions of major engineering elements, such as Al, known as γ' inducer, as well as Cr, serving as oxidation resistance enhancer, for a variety of Ni-base superalloys.[4–8] In particular, co-deposition of two or more elements in a controlled manner, considered to be technically challenging due to the differences in halide vapor pressures, has been successfully practiced in Al + Si,[9] Cr + Al,[10,11] and Al + Ti[12] systems. The addition of refractory metals, such as Mo, Ta, Re, and W, to Ni-base superalloys has been established to enhance solid solution strengthening, and, as a result, high-temperature creep resistance imparted by the slowed diffusion process of responsible element and the reduced kinetics of coarsening of γ', the strengthening phase determining the elevated temperature properties of the alloys. However, to our knowledge, only one article applies the pack cementation technology to depositing refractory metals,[13] despite its potential for creating advanced coatings. In this article, Li *et al.*[13] successfully implemented NH_4Cl-activated cementation to deposit Mo onto pure Ti substrate and form a Mo diffusion layer at temperatures from [1173 K to 1323 K (900 °C to 1050 °C)].

Cellular precipitation, often referred interchangeably as discontinuous precipitation or grain-boundary precipitation, has been extensively documented in various alloy systems,[14–16] and, in particular, in many nickel-base superalloys.[17–25] Reactions of such category generally result in the formation of multi-phase cellular structure. This type of phenomenon is of significance to the development of certain Ni-base superalloy grades, as the formation of cellular structures may be accompanied by the presence of detrimental topologically closed packed (TCP) phases.[20,22] Supersaturation of refractory solute atoms, such as Re, Mo, or W, in the γ matrix has been suggested as the driving force facilitating the precipitation of cellular structures and TCP phases. Additionally, Nolfi's model has been adapted for the case of a migrating reaction interface, where the solute transport is controlled by short-circuit-type grain-boundary diffusion.[24] Cellular precipitation is also favored under conditions of high plastic deformation.[25]

CONG WANG, Professor, formerly with the Department of Materials Science and Engineering, Northwestern University, Evanston, IL 60208, is now with the College of Materials and Metallurgy, Northeastern University, Shenyang 110819, P.R. China. Contact e-mail: wangc@smm.neu.edu.cn DAVID C. DUNAND, Professor, is with the Department of Materials Science and Engineering, Northwestern University.

Manuscript submitted July 31, 2014.
Article published online March 12, 2015

However, other researchers argue that cellular structures could simply be eutectic phases made possible through incipient melting due to the local segregation of solute atoms.[26–31]

In this letter, we showcase the microstructural development of Ni-Cr wires subjected to pack cementation, during which Al + Ti co-deposition as well as Mo diffusion is demonstrated, leading to the creation, after homogenization, of Ni-Cr-Al-Ti and Ni-Cr-Mo-Al-Ti alloys with superalloy compositions and $\gamma + \gamma'$ structures. Moreover, we report the formation of unexpected cellular structures, which are formed along the phase boundaries between γ matrix and primary γ' grains. We argue that the cellular structures are eutectic $\gamma + \gamma'$ phases, and postulate that the occurrence of this unusual phenomenon is due to incipient melting.

II. EXPERIMENTAL PROCEDURES

A. *Pack Cementation*

Raw materials employed in this study were procured from Alfa Aesar and include: Ni-Cr wires (Ni-20Cr-1Si-0.5Fe, wt pct) with a diameter of 143 μm as substrate; Al_2O_3 powder (20 to 50 μm particle size) as inert filler; NH_4Cl powder (100 μm particle size) as halide source; and metal sources, *i.e.*, Mo powder (2 to 7 μm particle size), Ni-70 at. pct Al powders (150 μm particle size), or pure Ti powders (44 μm particle size).

Pack cementation experiments were carried out in a tube furnace under continuous argon flow at 1273 K (1000 °C). Detailed procedures can be found elsewhere.[2,32] Two types of alloys, namely, Ni-Cr-Al-Ti and Ni-Cr-Mo-Al-Ti, were created.

For the Ni-Cr-Al-Ti alloy, Al and Ti were co-deposited for 10 min from a pack composed of 3 wt pct NH_4Cl, 30 wt pct Ni-70 at. pct Al, 10 wt pct Ti, and 57 wt pct Al_2O_3. For the Ni-Cr-Mo-Al-Ti alloy, Mo pack cementation took place first, with replenished feedstock (3 wt pct NH_4Cl, 40 wt pct Mo, and 57 wt pct Al_2O_3) at 1-hour interval, for eight cycles, to ensure sufficient supply of Mo, which is a slow diffuser. Subsequently, the Mo-alloyed wires were homogenized at 1373 K (1100 °C) for 48 hours under high vacuum, terminated by fast cooling. Following this step, alumotitanization was carried out for 10 minutes with the same pack as the first alloy.

For both alloys, after Al and Ti co-deposition, the wires were homogenized at 1373 K (1100 °C) for 24 hours under high vacuum furnace, to eliminate Al and Ti concentration gradients, and to induce the $\gamma + \gamma'$ superalloy structure upon aging. This final step was performed at 1173 K (900 °C) for 12 hours and also terminated by fast furnace cooling.

B. *Characterization*

Specimens were mounted in epoxy, then ground and polished down to 0.05 μm colloidal alumina by standard metallographic procedures. Selected polished cross-sections were etched by a solution composed of 33 vol pct DI water, 33 vol pct nitric acid, 33 vol pct acetic acid, and 1 vol pct hydrofluoric acid, which preferentially attacks γ'.[2] The microstructure was investigated by a Hitachi SU8030 scanning electron microscope (SEM) at an acceleration voltage of 15 kV. Compositional analysis was completed with an energy dispersive X-ray spectrometer (EDS) within the SEM. The EDS signal was calibrated by standard samples of Ni with accuracy of ±1 pct.

III. RESULTS AND DISCUSSION

A. *Microstructure Development of Ni-Cr-Al-Ti and Ni-Cr-Mo-Al-Ti Alloys*

Figures 1 and 2 show series of SEM micrographs illustrating the microstructure development of the Ni-Cr-Al-Ti (Figures 1(a) through (f)) and Ni-Cr-Mo-Al-Ti (Figures 2(a) through (f)) wires, respectively.

Starting from Ni-Cr wires, the Ni-Cr-Al-Ti alloy was achieved by Al + Ti co-deposition, the effect of which is shown in Figure 1(a). From the cross-sectional view, a ~10 μm thick, uniform coating layer has been created. Higher magnification view of the coating in Figure 1(b) reveals that it is composed of three distinctive layers. Based on EDS phase composition and comparison with similar results,[2,33] they are determined to be: (i) an outer shell with a stoichiometry close to Ni_2AlTi, the β' phase, (ii) an intermediate shell with $Ni_3(Al,Ti)$ composition, which is primary γ' (denoted as γ_p') phase, and (iii) an inner shell where Cr was rejected by the other shells and precipitated in the Ni-Cr matrix. This inner shell, which is about 5 μm wide, is shown in Figure 1(c) after deep etching, and shows α-Cr rods growing radially in the direction of the diffusion flux. The rods have length and width ranging from 0.6 to 2 μm and from 0.3 to 0.5 μm, respectively. The multi-shell structure of the Ti-Al cementation coating presented here is consistent with findings from previous studies.[2,12,34]

Figure 1(d) depicts a representative cross-sectional view of the Al + Ti-coated Ni-Cr wire after homogenization at 1373 K (1100 °C) for 24 hours. It is apparent that the three-shell structure disappears and that a featureless microstructure prevails, indicating a uniform distribution of Al and Ti within a Ni-Cr matrix. EDS results obtained from an area analysis from the core region confirms that the wire contains 1.2 ± 0.4 wt pct Al and 3.5 ± 0.7 wt pct Ti, the combination of which is known to induce the formation of $\gamma + \gamma'$ structures. Further etching brings along more details of this sample as illustrated in Figure 1(e). It is found that the vast majority of the cross section remains intact but the outer shell, composed mainly of γ_p', has been etched down and become serrated in selected regions. Most importantly, a closer examination into the matrix unveils the desired $\gamma + \gamma'$ superalloy structure as illustrated in Figure 1(f), where the cuboidal γ' precipitates ranging from 10 to 50 nm in size are shown to distribute evenly in the γ matrix. Such fine γ' phases are believed to be secondary precipitates (denoted as γ_s') as the homogenization temperature [1373 K (1100 °C)] is

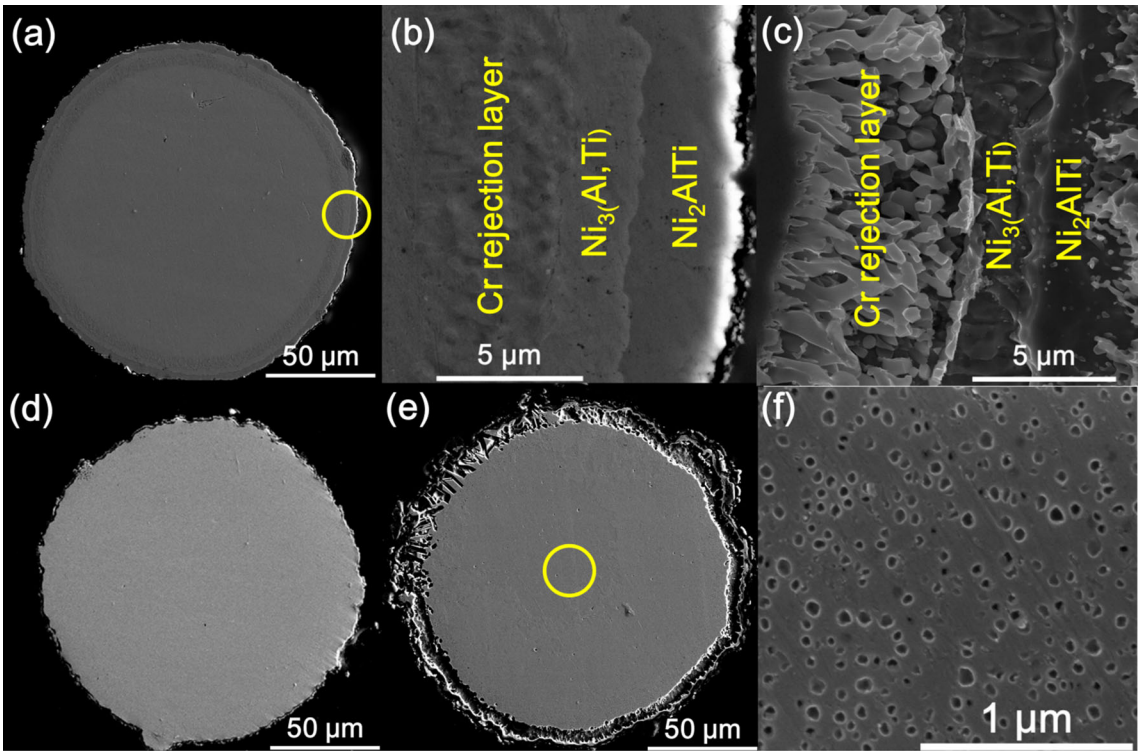

Fig. 1—Series of SEM micrographs showing the microstructure development in cross sections of Ni-Cr-Al-Ti during and after pack cementation. (*a*) Ni-Cr wire after Al + Ti co-deposition, (*b*) enlarged illustration of coated area circled in (a) with three distinctive layers present on the Ni-Cr wire, consisting of an outer shell of Ni2AlTi, a middle shell of Ni3(Al,Ti), primary γ', and an inner Cr rejection layer, (*c*) same three-layer structure as in (b) but after etching showing the elongated shape of the α-Cr precipitates, (*d*) Ni-Cr-Al-Ti wire after homogenization, (*e*) homogenized Ni-Cr-Al-Ti wire (same as in (d)) after etching showing the serrated boundary between the γ' outer shell and $\gamma + \gamma'$, and (*f*) representative $\gamma + \gamma'$ superalloy structure present in the etched Ni-Cr-Al-Ti wire core region circled in (e).

below (but close to) the solvus temperature of the alloy.[35]

The Ni-Cr-Mo-Al-Ti alloy was created with Mo being first introduced into the Ni-Cr wire by deposition and homogenization, followed by Al + Ti co-deposition and homogenization. After the Mo pack cementation step, as demonstrated in Figure 2(a), the cross section of the Ni-Cr wire contains large amounts of Kirkendall pores, which grow steadily as the Mo supply is replenished at 1-hour intervals, up to 8 hours. The Kirkendall pores result from imbalanced diffusional fluxes, with a net outward flux of Ni and Cr atoms leaving vacancies in the Ni-Cr matrix, which coalesce into pores.[36–38] After homogenization at 1373 K (1100 °C) for 48 hours, as shown in Figure 2(b), the central part of the wire is pore-free indicating pore sintering, while the outer wire region is characterized by the Kirkendall pores merging into larger, elongated pores which are connected at the wire surface. Mo content, as measured by EDS, is 4.5 ± 0.7 wt pct and near uniform throughout the entire cross-section. Subsequent Al + Ti co-deposition of the Ni-Cr-Mo alloy yields a uniform three-layer coating (Figure 2(c)), with a structure similar to that shown in Figures 1(b) and (c) for the Mo-free wires. Further homogenization at 1373 K (1100 °C) for 24 hours allows the Al (1.8 ± 0.4 wt pct) and Ti (2.5 ± 0.6 wt pct) to become uniformly across the wire volume, as verified by EDS and shown in Figure 2(d). Again, large Kirkendall pores are present. After etching, the Ni-Cr-Mo-Al-Ti alloy shows a differentiated structure, shown in Figure 2(e), with an outer shell of (γ_p') grains, about 16 μm in width, surrounding an inner core having a uniform superalloy composition of Ni-17.9Cr-4.5Mo-1.9Al-2.5Ti (wt pct). An enlarged micrograph of the inset circled in Figure 2(e) shows the expected $\gamma + \gamma'$ superalloy structure, as illustrated in Figure 2(f), which is nearly identical to that of the Ni-Cr-Al-Ti alloy shown in Figure 1(f). It is noted that Kirkendall pore density might not be distributed uniformly along the wire length, as the cross section in Figure 1(c) shows much fewer pores as compared to its counterparts before and after further treatment.

B. *Cellular Structures*

As evidenced in Figures 1(e) and 2(e), for both the etched Ni-Cr-Al-Ti and Ni-Cr-Mo-Al-Ti wires, their outer shells are composed of γ_p' grains. Areas of interests are represented by the inset circles in the cross-sectional views in Figures 3(a) and (d), and corresponding high magnification images of each region are highlighted in Figures 3(b) and (c), (e) and (f), for Ni-Cr-Al-Ti and Ni-Cr-Mo-Al-Ti, respectively.

These and numerous other observations of the etched outer shell region reveal that cellular structures are present along planar interfaces that form an angle with

the plane of polish. Because the etchant employed in the present experiments preferentially dissolves the γ' phase in the alloy, it can be deduced that cellular structures are originally formed between phase boundary of the primary γ_p' and the γ matrix (also containing secondary γ' fine precipitates). As a result of etching, the γ_p' grains are chemically dissolved and therefore show a surface which is under the plane of polish on which the adjacent, unetched γ matrix grains are present. The phase boundary between the remaining γ grains and the removed volume of the γ_p' grains are thus made visible in two-dimensions rather than in one-dimension grain-boundary line in unetched samples where phase grains are on the same plane polish. These phase boundaries are often decorated by a cellular structure, which show an abrupt end in Figures 3(b, c, e, f) where they intersect the unetched γ grains in the plane of polish and also with the surface of the deep etched γ_p' grains, parallel to, but under, the plane of polish. EDS analysis shows that phase boundaries decorated with cellular structures exhibit essentially the same average composition as the bulk γ matrix. It is thus plausible to infer that cavities within the cellular structures are the sites originally filled with fine, nanometric γ' precipitates, which are confined to the phase boundary and grow only up to ~100 nm into the γ grain, as shown in the top array of the cellular structures (shown by the red rectangular in Figure 3(e)). The struts of the cellular structures consist then of unetched γ phase which is separated the γ' precipitates. The volume fraction of γ' in the cellular structure is high, which is consistent with a $\gamma + \gamma'$ structure resulting from eutectic reactions.

Extensive observations of the cellular structures indicate that they are present only on selected phase boundaries. Figure 3(e) illustrates this observation, with one side of the γ grain interface being fully decorated by the cellular structure and the other side being featureless. Furthermore, the cellular structure appears to be highly ordered but not perfectly periodic, implying it was produced by interdiffusion of major elements as opposed to phase separation of a solid solution. Lack of long-range periodicity is characterized by the concurrent presence of perfect and imperfect arrays, as showcased by the dashed regions in Figure 3(f).

Representative cellular structures from the Ni-Cr-Mo-Al-Ti alloy are presented in Figure 4, which shows patterns that are reminiscent of spider webs (Figure 4(a)), honeycombs (Figure 4(b)) and fly wings (Figure 4(d)), or show lamellar morphology (Figure 4(c)). Cavity size from the network-like structures (Figures 4(a), (b), and (d)) and the spacing between lamellar arrays (Figure 4(c)) are ranging from 50 to 200 nm. Compositional analysis on cellular structures shows negligible difference as compared to that of the γ matrix, confirming the absence of γ' precipitates expected from the deep chemical etching used here.

Adjacent cellular structures may encompass a variety of defined patterns. Figure 5 shows a collection of micrographs from the Ni-Cr-Mo-Al-Ti alloy combining distinguishable patterns as illustrated in Figure 4. Based on these morphological definitions, for instance, Figures 5(a) and (c) are examples of adjacent honeycomb and lamellar patterns, while Figure 5(b) shows spider-web, honeycomb, and lamellar configuration in close proximity of each other.

Literature descriptions of precipitated cellular structures are divided into two major groups. One leading approach, largely known as discontinuous (cellular) precipitation, advocates the theory of decomposition of a supersaturated original phase into structurally identical yet solute-depleted matrix and newly created precipitates along moving grain boundaries. Reactions based on this mechanism promote the formation of multi-phase cellular structure.[14,16] As far as superalloy families are concerned, cellular precipitation has been reported, but not for the γ' phase, but rather for TCP phases (including η phase[39] and P phase[20,22,40]), or for MC carbides[41,42] that are randomly arranged at grain boundaries. Inherent phase transformations will be largely driven by the high degree of supersaturation of responsible refractory metals, such as W, Mo, and Re. Along this argument, the supersaturated γ matrix will react with the γ' precipitate, leading to the formation of γ' matrix and γ precipitates and TCP phases.[22]

However, the two essential requirements, *i.e.*, the supersaturation of refractory metals, and the ensuing formation of TCP phases, are not met for our Ni-Cr-Al-Ti wires which are free of refractory metals (Sect. II–A). Although the Ni-Cr-Mo-Al-Ti alloys have a final composition of 4.5 wt pct Mo, which is the only refractory metal element present, nearly identical cellular structures are also observed in Ni-Cr-Al-Ti wires, indicating that Mo is not necessary for the formation of cellular structures. Moreover, there is no experimental evidence that any TCP phases, characteristic of the above-mentioned reaction mechanism, are formed in our Ni-Cr-Al-Ti and Ni-Cr-Mo-Al-Ti wires. In addition, EDS analysis reveals no appreciable chemical difference between the cellular structure and the bulk γ matrix, and no significant depletion of solute along the vicinity of phase boundaries, so the driving force from chemical potential difference for precipitate nucleation is not present.

The other mechanism put forward in the literature for *in situ* cellular structures is not based on the idea that these cellular structures result from a solid-state precipitation event, but rather invoke a solidification mechanism, induced by incipient melting due to local solute segregation.[26–31] Through a differential thermal analysis on the effect of alloying elements (Al, Ti, Ta, *etc.*) on incipient melting temperatures during solidification, Sponseller[43] reported incipient melting of Inconel 718 occurring at 1403 K (1130 °C) and the presence of cellular $\gamma + \gamma'$ eutectic. The author further reported that segregation of Ti might contribute to the significant decrease of the incipient melting point. In a parallel study, Zhu *et al.*[27] observed that liquid phase adjacent to $\gamma + \gamma'$ eutectic nodules could persist at temperatures as low as 1373 K (1100 °C) (our homogenization temperature) in slowly solidified IN738. Zhou *et al.*[28] reported that, during solidification of CM247 and CMSX-4 alloys, continuous $\gamma + \gamma'$ eutectic films are formed along grain boundaries due to segregated Al and Ta in the interdendritic region. Finally, in

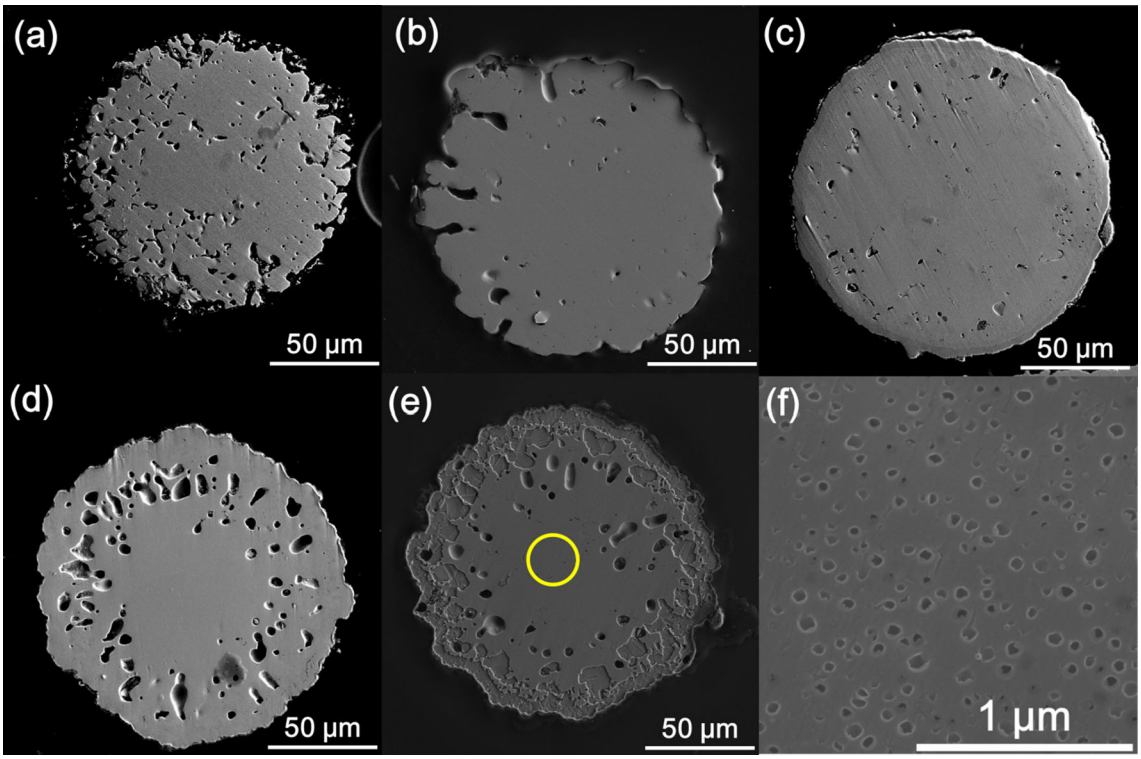

Fig. 2—Series of SEM micrographs showing the microstructure development in cross-sections of Ni-Cr-Mo-Al-Ti wires during and after pack cementation. (*a*) Ni-Cr wire after 8 h Mo deposition with extensive presence of Kirkendall pores, (*b*) Ni-Cr-Mo wire after homogenization, with reduced porosity in the central wire region, (*c*) Ni-Cr-Mo wire after Al + Ti co-deposition (with the same three layers as in (a through c)), (*d*) Ni-Cr-Mo-Al-Ti wire after homogenization showing extensive porosity, (*e*) homogenized Ni-Cr-Mo-Al-Ti wire (same as in (d)) after etching showing serrated boundary between the γ' outer shell and $\gamma + \gamma'$, and (*f*) $\gamma + \gamma'$ superalloy structure obtained from the etched Ni-Cr-Mo-Al-Ti wire core region, inset circled in (e).

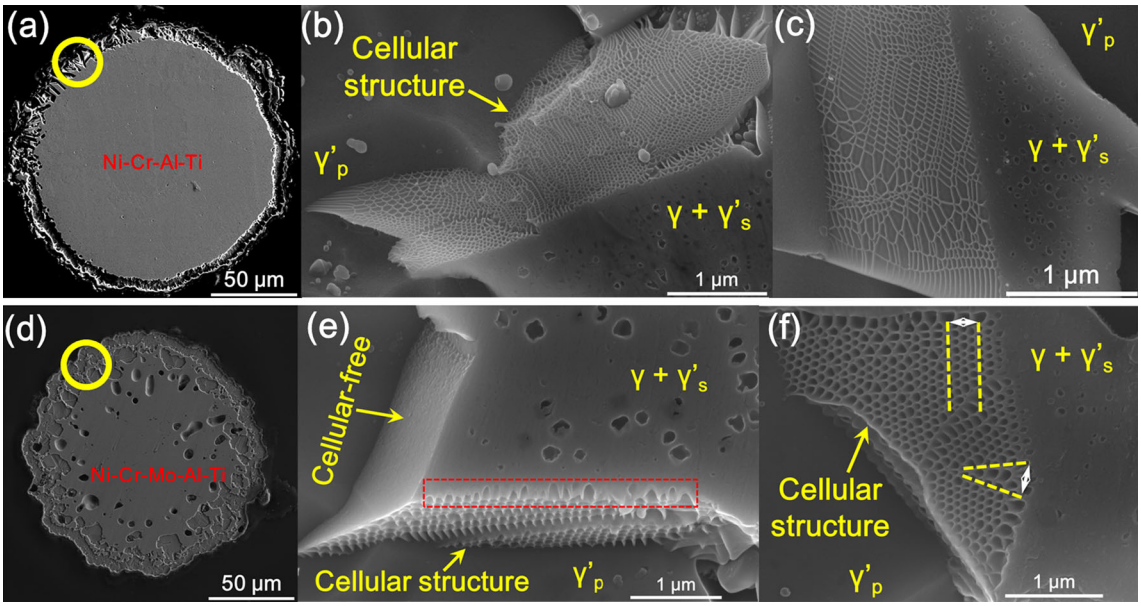

Fig. 3—SEM micrographs showing (*a*) cross-section of etched Ni-Cr-Al-Ti (homogenized) wire, (*b*, *c*) higher magnification view within wire outer region circled in (a), showing primary γ' phase (noted as γ_p'), γ phase grains containing secondary γ' precipitates (noted as γ_s'), and cellular structure at boundary between γ grain (unetched) and primary γ' (partially etched), (*d*) cross section of etched Ni-Cr-Mo-Al-Ti (homogenized) wire, (*e-f*) higher magnification view within wire outer region circled in (d), showing the same features as in (b, c). In (f), both perfect and imperfect arrays are highlighted by the dashed lines.

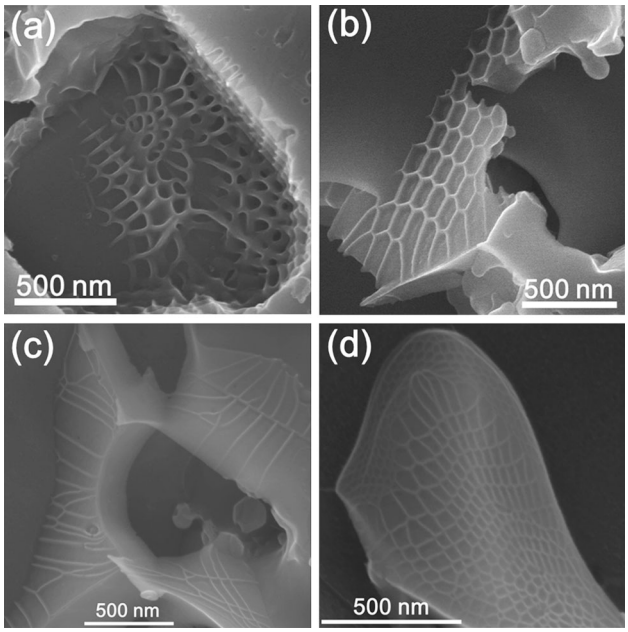

Fig. 4—SEM micrographs showing characteristic patterns of cellular structures obtained from the Ni-Cr-Mo-Al-Ti alloy. (*a*) Spider-web, (*b*) honeycomb, (*c*) lamellar, and (*d*) fly-wing.

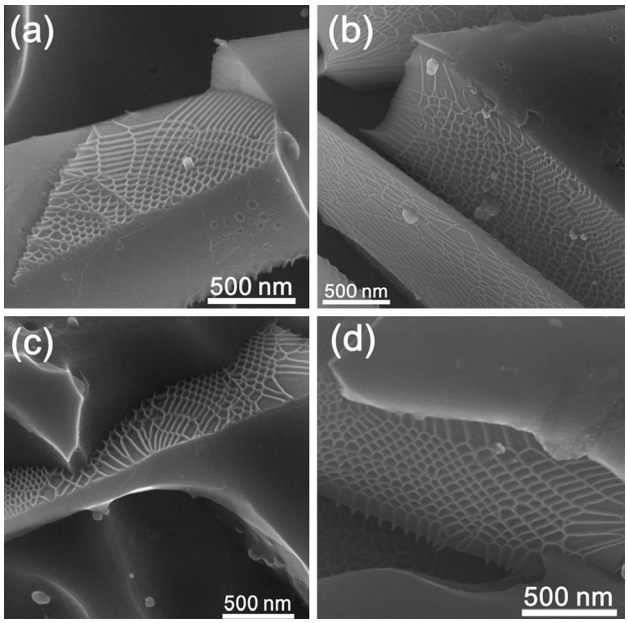

Fig. 5—SEM micrographs of cellular structures from the Ni-Cr-Mo-Al-Ti alloy showing the appearance of distinct patterns formed adjacent to each other. (*a*) honeycomb + lamellar, (*b*) honeycomb + lamellar + spider-web, (*c*) honeycomb + lamellar, and (*d*) honeycomb + lamellar + spider-web.

a study on the effect of heat-treatment parameters on solidification microstructures of GTD-111, Sajjadi *et al.*[29] observed that extended homogenization (2 to 4 hours) at 1473 K (1200 °C) would induce local melting of eutectic $\gamma + \gamma'$.

We favor the incipient melting induced eutectic hypothesis as it shares common ground with our findings. To illustrate this argument, cellular structures of our Ni-Cr-Al-Ti and Ni-Cr-Mo-Al-Ti wires are collected in Figure 6 and compared with representative eutectic structures of commercial grade superalloys which experienced analogous processing history as our wires. Figures 6(a) and (b) show the "sun-flower" morphology, apparently similar to our spider-web structure (Figure 3(a)). As explicitly pointed out in Reference 26 from which Figure 6(b) is obtained, extensive "sun-flower" eutectic structures are created by incipient melting of CMSX-2 alloy. Figures 6(c) and (d) presents a direct comparison between our lamellar structure and a eutectic $\gamma + \gamma'$ created as a result of local melting in GTD-111.[29] The last group, Figure 6(e) and (f), illustrates the branching nature of γ walls separating the γ' precipitates, and strengthen the possibility that our lamellar structure is of the same type as the eutectic structure created as continuous films along grain boundaries, as suggested in Reference 28 for CM247.

A major difference is that the eutectic structures found in our wires have a significantly smaller, submicrometer (*i.e.*, nanometric) thickness than those from literatures. One possible reason is solid-state interdiffusion is operating in the present study while other investigations employed melting and bulk solidification.

As mentioned earlier, the volume fraction of γ' in the cellular structure is high, which is consistent with a $\gamma + \gamma'$ structure resulting from eutectic reactions. Had γ' phase precipitated during solid-state reactions, as proposed in the supersaturation-driven theory, its volume fraction could be as low as that of the secondary γ' precipitates in the bulk of the γ matrix (denoted as γ_s' in Figure 3).

Considering the similarities in the compositions of our wires and those cited in literature, and given the high homogenization temperature [1373 K (1100 °C)] and long homogenization time (24 hours) during which large scale diffusion of Al and Ti occurs from the surface of the wire to their interior, it is reasonable to infer that melting point depressors, presumably Ti and/or Si, may have segregated along phase boundaries and facilitated the occurrence of incipient melting, which results in a cellular structure composed of eutectic $\gamma + \gamma'$ during solidification. However, EDS analysis could not detect the putative solute segregation (Ti and/or Si) along phase boundaries as it is difficult to identify boundaries without etching, and the segregated films (~100 nm in thickness) are too narrow to be resolved by the use of conventional analysis techniques (SEM/EDS). Therefore, advanced characterization techniques, such as focused ion beam (FIB) combined with local-electrode atom-probe (LEAP), are called for to corroborate the segregation hypothesis.

The cellular eutectic structure occurring in the superalloys may have engineering or industrial implications. It is well known that a high volume fraction of the eutectic would degrade the mechanical properties in a superalloy because of the production of γ'-deficient regions. Therefore, a method to prevent these cellular structures will be reported elsewhere.[44] On the other hand, the high volume fraction and the fine size of the γ' precipitates may in fact prevent phase boundary sliding

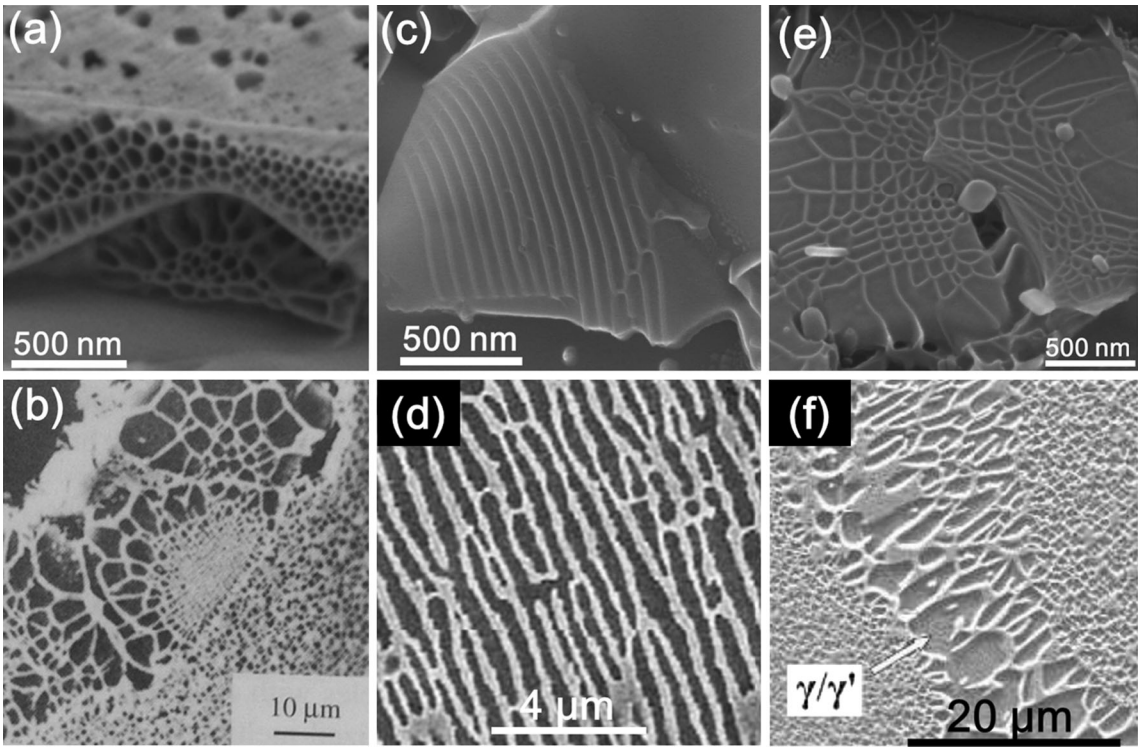

Fig. 6—Eutectic features observations in this study on homogenized wires (*a*, *c*, *e*) are compared with similar features from literature (*b*, *d*, *f*). (a) and (b) are ''sunflower'' structure from the Ni-Cr-Mo-Al-Ti wire compared with CSMX-4 from Ref. [23]; (c) and (d) are lamellar structure from the Ni-Cr-Al-Ti wire compared with GTD-111 from Ref. [26]; (e) and (f) are branching networks from the Ni-Cr-Al-Ti wire compared with CM247 from Ref. [25].

and improve creep resistance. Mechanical testing of wires is needed to test these hypotheses, but is beyond the scope of the present article.

IV. SUMMARY

In this study, pack cementation has been employed to simultaneously add Al and Ti as coatings to Ni-Cr wires, resulting in homogenous Ni-Cr-Al-Ti composition after homogenization; upon subsequent aging, the wires consists of γ grains containing nanometric γ' precipitates typical of Ni-base superalloys. An intermediate step of Mo pack cementation results in a Ni-Cr-Mo-Al-Ti superalloy with $\gamma + \gamma'$ microstructure. Mo deposition however promotes the occurrence of Kirkendall pores.

Cellular structures consisting of a single layer of interconnected struts are observed to form along selected phase boundaries between γ grains and large primary γ' grains near the Al-rich wire surfaces. Based on various microstructural features, *i.e.*, ordered but not periodic structure, localization of occurrence at phase boundaries, as well as lack of topologically close-packed phases, and based on comparison with literature, it is concluded that the present cellular structure is composed of eutectic $\gamma + \gamma'$ created by incipient melting and subsequent solidification of a thin film with high solute segregation, created during homogenization of the wires.

ACKNOWLEDGMENTS

The authors acknowledge the financial support from the Defense Advanced Research Projects Agency under the Contract Number of W91CRB1010004 monitored by Dr. Judah Goldwasser (Program Manager). They also thank Dr. Dinc Erdeniz and Ms. Ashley Paz y Puente (both of Northwestern University) for useful discussions.

REFERENCES

1. R. Mévrel, C. Duret, and R. Pichoir: *Mater. Sci. Tech.*, 1986, vol. 2, pp. 201–06.
2. D. Erdeniz and D.C. Dunand: *Intermetallics*, 2014, vol. 50, pp. 43–53.
3. D.C. Dunand, A.M. Hodge, and C. Schuh: *Mater. Sci. Technol.*, 2002, vol. 18, pp. 326–32.
4. G.W. Goward and D.H. Boone: *Oxid. Met.*, 1971, vol. 3, pp. 475–95.
5. A.J. Hickl and R.W. Heckel: *Metall. Trans. A*, 1975, vol. 6A, pp. 431–40.
6. J.R. Rairden and M.R. Jackson: *J. Vac. Sci. Technol.*, 1980, vol. 17, pp. 77–80.
7. A.M. Hodge and D.C. Dunand: *Intermetallics*, 2001, vol. 9, pp. 581–89.
8. A.E. Simmons: U.S. Patent 3,649,225, 1972.
9. Z.D. Xiang and P.K. Datta: *Mater. Sci. Eng. A*, 2003, vol. 356, pp. 136–44.
10. R. Bianco and R.A. Rapp: *J. Electrochem. Soc.*, 1993, vol. 140, pp. 1181–90.
11. W. Da Costa, B. Gleeson, and D.J. Young: *J. Electrochem. Soc.*, 1994, vol. 141, pp. 1464–71.

12. D. Erdeniz, K.W. Sharp, and D.C. Dunand: Unpublished research, 2015.
13. J. Li, C. Xia, and Y. Gu: *J. Cent. South Univ.*, 2004, vol. 11, pp. 15–18.
14. R.A. Fournelle and J.B. Clark: *Metall. Trans.*, 1972, vol. 3, pp. 2757–67.
15. D.B. Williams and E.P. Butler: *Inter. Met. Rev.*, 1981, vol. 3, pp. 153–83.
16. F. Findik: *J. Mater. Sci. Lett.*, 1998, vol. 17, pp. 79–83.
17. C.Y. Barlow and B. Ralph: *J. Mater. Sci.*, 1979, vol. 14, pp. 2500–08.
18. J.V. Wood, P.F. Mills, J.K. Bingham, and J.V. Bee: *Metall. Trans. A*, 1979, vol. 10A, pp. 575–64.
19. W.S. Walston, J.C. Schaeffer, and W.H. Murphy: *Superalloys*, 1996, pp. 9–18.
20. J.D. Nystrom, T.M. Pollock, W.H. Murphy, and A. Garg: *Metall. Mater. Trans. A*, 1997, vol. 28A, pp. 2443–52.
21. M. Sakaguchi and M. Okazaki: *J. Soc. Mat. Sci. Japan*, 2005, vol. 54, pp. 122–29.
22. A. Heckl, S. Cenanovic, M. Goken, and R.F. Singer: *Metall. Mater. Trans. A*, 2012, vol. 43A, pp. 10–19.
23. M.F. Henry, Y.S. Yoo, D.Y. Yoon, and J. Choi: *Metall. Trans. A*, 1992, vol. 24A, pp. 1733–43.
24. H. Loyer Danflou, M. Macia, T.H. Sanders, and T. Khan: *Superalloys,* 1996, pp. 119–27.
25. R. Burgel, P.D. Portella, and J. Preuhs: *Superalloys*, 2000, pp. 229–38.
26. M Durand-Charre: *The Microstructure of Superalloys*, CRC Press, Boca Raton, FL, 1998.
27. Y. Zhu, S. Zhang, T. Zhang, J. Zhang, Z. Hu, X. Xie, and C. Shi: *Superalloys*, 1992, pp. 145–54.
28. Y. Zhou, A. Volek, and R.F. Singer: *J. Mater. Res.*, 2006, vol. 21, pp. 2361–70.
29. S.A. Sajjadi, S.M. Zebarjad, R.I.L. Guthrie, and M. Isac: *J. Mater. Proc. Technol.*, 2006, vol. 175, pp. 376–81.
30. Y. Xie and M. Wang: *Surf. Coat. Technol.*, 2006, vol. 201, pp. 691–98.
31. X. Huang, Y. Kang, H. Zhou, Y. Zhang, and Z. Hu: *Mater. Lett.*, 1998, vol. 36, pp. 210–13.
32. C. Wang and D.C. Dunand: *Metall. Mater. Trans. A*, 2014, vol. 45A, pp. 6252–59.
33. R. Yang, J.A. Leake, and R.W. Cahn: *J. Mater. Res.*, 1991, vol. 6, pp. 343–54.
34. D.C. Tu and L.L. Siegle: *Thin Solid Films*, 1982, vol. 95, pp. 47–56.
35. W.T. Loomis, J.W. Freeman, and D.L. Sponseller: *Metall. Trans.*, 1972, vol. 3, pp. 989–1000.
36. C.P. Heijwegen and G.D. Rieck: *Acta Metall.*, 1974, vol. 22, pp. 1269–1281.
37. V.D. Divya, S.S.K. Balam, U. Ramamurty, and A. Paul: *Scripta Mater.*, 2010, vol. 62, pp. 621–24.
38. T.C. Chou and L. Link: *Scripta Mater.*, 1996, vol. 34, pp. 831–38.
39. T. Takahashi, T. Ishiguro, K. Orita, J. Taira, T. Shibata, and S. Nakato: *Superalloys*, 1994, pp. 557–65.
40. T.M. Pollock: *Mater. Sci. Eng. B*, 1995, vol. 32, pp. 255–66.
41. A.K. Koul and R. Thamburaj: *Metall. Trans. A*, 1985, vol. 16A, pp. 17–27.
42. H.M. Tawancy: *J. Mater. Sci.*, 1992, vol. 27, pp. 6481–89.
43. D.L. Sponseller: *Superalloys*, 1996, pp. 259–70.
44. C. Wang and D.C. Dunand: *Metall. Mater. Trans. A*, in press.